NUMERICAL SIMULATION STUDY ON FALLING-FILM EVAPORATION OF MOLASSES ETHANOL WASTEWATER
/
甘蔗糖蜜酒精废水降膜蒸发的数值模拟研究

Liang WANG[1,3#] Mingzhe HU[2#] Xiaole WANG[2*]
[1)]College of Energy and Architectural Engineering, Shandong Huayu University of Technology, Dezhou 253023, China;
[2)]School of Thermal Engineering, Shandong Jianzhu University, Jinan, Shandong 250101, China;
[3)]Shandong Engineering Research Center of Low-Carbon Energy Internet of Things Technology, Dezhou, 253023, China;
Tel:13406930176; E-mail: Wang24215@163.com
DOI: https://doi.org/10.35633/inmateh-79-76

***Keywords:** Falling-film evaporation, molasses ethanol wastewater, VOF method, Lee phase-change model, Liquid film thickness, Heat transfer coefficient*

ABSTRACT
To investigate the concentration of molasses ethanol wastewater, a two-dimensional numerical model of falling-film evaporation over horizontal tubes was developed. The model used the Volume of Fluid (VOF) method to capture the liquid-gas interface and was coupled with the Lee phase-change model. The model was validated by comparing the predicted liquid-film thickness and average heat-transfer coefficient with experimental data reported in the literature. The validated model was then used to systematically investigate the effects of spray density (0.10 ~ 0.30 kg/(m·s)) and heat-transfer temperature difference (2 ~ 8 °C) on the falling-film flow and evaporation performance of molasses ethanol wastewater. The results showed that the liquid-film thickness initially decreased and subsequently increased along the circumferential direction, reaching a minimum within the angular range of 90° ~ 120°. Increasing the spray density produced a thicker liquid film; nevertheless, the average heat-transfer coefficient increased monotonically by 23.0% ~ 27.2%, whereas the mass-transfer rate decreased by 19.3% ~ 25.1%. Increasing the heat-transfer temperature difference increased both the average heat-transfer coefficient and the mass-transfer rate. When the temperature difference increased from 2 to 8 °C, the mass-transfer rate increased 2.84 ~ 3.07-fold, and its effect on evaporation performance was substantially greater than that of spray density. Therefore, where operating conditions permit, a lower spray density combined with a higher heat-transfer temperature difference is recommended for the falling-film evaporative concentration of molasses ethanol wastewater.

摘要
为了处理糖蜜酒精废液的浓缩问题，基于流体体积法（VOF）和 Lee 相变模型，针对水平管外的降膜蒸发过程建立了一个二维数值模型。首先，通过将模拟得到的液膜厚度和平均传热系数与文献实验数据对比，验证了模型的可靠性。随后，利用已验证的模型系统研究了喷淋密度（0.10 ~ 0.30 kg/(m·s)）和传热温差（2~8 ℃）对糖蜜酒精废液降膜流动与蒸发性能的影响。结果表明：液膜厚度沿周向先减小后增大，在 90°~120°的圆周角范围内达到最小值。喷淋密度增大使液膜变厚，但平均传热系数单调上升（增幅为 23.0% ~ 27.2%），而质量传递速率则下降了 19.3% ~ 25.1%。提高传热温差同时增大了平均传热系数和质量传递速率。值得注意的是，当温差从 2℃升至 8 ℃时，质量传递速率增大了 2.84 ~ 3.07 倍，其对蒸发效率的影响远超喷雾密度。因此，建议在糖蜜酒厂废水的降膜蒸发浓缩过程中，在条件允许的情况下，可以采用低喷雾密度与高温差相结合的操作策略。

INTRODUCTION
Molasses ethanol wastewater is a high-strength organic effluent discharged during the fermentation of sugarcane molasses for alcohol production.

It is principally characterized by exceedingly high chemical oxygen demand, pronounced viscosity, intense coloration, and an abundance of suspended solids and dissolved organic matter (*Li et al., 2022*).

 # Liang Wang and Mingzhe Hu contributed equally to this work

In China, the cane molasses alcohol industry generates millions of tons of such wastewater annually, which, if discharged directly without adequate treatment, would provoke severe ecological consequences, such as eutrophication of water bodies and soil acidification accompanied by compaction, while concurrently representing a colossal waste of organic resources (*Chowdhary et al., 2018*). Among the various concentration techniques, falling-film evaporation is regarded as a comparatively definitive treatment strategy, owing to its small driving temperature difference, high heat transfer coefficient, compact equipment footprint, and compatibility with low-temperature heat sources (*Wang et al., 2026*).

A considerable body of research has examined the distribution of liquid film thickness during the falling-film process (*Wang et al., 2026*). Although increasing the tube spacing promotes falling-film evaporation, an excessively large spacing adversely affected the overall volume of the falling-film evaporator; therefore, elucidating the influence of tube spacing on film thickness could contribute to enhancing evaporator compactness while preserving its thermal performance (*Tahir et al., 2019*). *Ibrahim et al.* (*2020*) reported that, at a Reynolds number of 574, increasing the tube spacing from 10 mm to 40 mm reduced the film thickness by 26%. Moreover, investigations have revealed that the liquid film was circumferentially non-uniform. Nusselt (1916) indicated that the film thickness is symmetric about the circumferential angle of 90° and followed a trend of initially decreasing and subsequently increasing along the circumferential direction. For circumferential angles between 0° and 90°, the resultant tangential component of gravity consistently outweighed the viscous force, causing the film flow velocity to rise and the film thickness to diminish with increasing circumferential angle (*Qiu et al., 2015*). As the circumferential angle further increased, the viscous force progressively intensified, whereas the combined contribution of the tangential gravity component and the inertial force gradually diminished (*Zhao et al., 2018*). Within the circumferential angle range of 90° to 120°, the tangential gravity component, the inertial force, and the viscous force attained mutual equilibrium. Under these conditions, the circumferential film thickness reached its minimum (*Zhang et al., 2020*).

Relevant scholars have noted that, in horizontal-tube falling-film evaporators, the falling-film heat transfer coefficient is merely 50%–80% of the in-tube condensation heat transfer coefficient (*Dai et al., 2022*); consequently, augmenting the falling-film heat transfer coefficient constitutes the key to intensifying falling-film evaporator performance. Under convection-dominated regimes, three distinct academic viewpoints have emerged concerning the effect of spray density on horizontal-tube falling-film evaporation (*Ubara et al., 2021*): (1) The heat transfer coefficient increased with rising spray density (*Qi et al., 2010*). For example, *Chen et al. (1997)* experimentally demonstrated that the average Nusselt number increased with the Reynolds number over the range 800 < Re < 4000. (2) As the spray density increased, the heat transfer coefficient initially decreased and then increased (*Su and Ouyang, 2019*). (3) No clear correlation was observed between the heat-transfer coefficient and spray density (*Gong, 2017*).

Considerable research has also investigated the effects of fluid properties on heat transfer during falling-film evaporation. However, most studies have focused on applications such as seawater desalination, alcohol concentration, refrigeration, and air conditioning, and have primarily measured falling-film heat-transfer coefficients for fluids such as pure water *(Liu et al., 2021)*, brine *(Gong et al., 2016)*, and halocarbon refrigerants *(Jin et al., 2019)*. Consequently, systematic investigations on high-viscosity, complex organic fluids such as molasses distillery wastewater remain scarce, and their falling-film flow and heat transfer behaviors are poorly understood. To fill this knowledge gap, the present study adopted molasses ethanol wastewater as the working fluid. The Volume of Fluid (VOF) method was introduced to track the gas-liquid interface and was coupled with the Lee evaporation phase-change model, thereby establishing a mathematical framework for the falling-film evaporation of molasses ethanol wastewater. The reliability of the numerical model was verified by comparing the predicted liquid film thickness and heat transfer coefficient with experimental data reported in the published literature (*Jia, 2025; Parken et al., 1990*), rather than through experiments conducted in the present study. The local distributions of the liquid film thickness and the heat transfer coefficient during the evaporation of this high-viscosity fluid were analyzed, and the variation patterns of the Nusselt number together with local and average heat transfer coefficients were systematically examined. The findings were anticipated to provide both a theoretical basis and a numerical predictive tool for the design of falling-film evaporators intended for molasses ethanol wastewater, while simultaneously enriching the numerical research methodology applicable to the evaporation and concentration of high-viscosity, complex liquid feeds.

MATERIAL AND METHODS

Physical model and meshing

Molasses ethanol wastewater was uniformly sprayed onto the outer surface of a horizontal tube through a liquid distributor, forming a thin and even liquid film. As the film spreads, it absorbs the latent heat released by the condensation of steam inside the horizontal tube and subsequently evaporates (*Jia, 2025*). Due to the symmetry of the horizontal tube structure, only the half-tube region between adjacent dropping points is modeled to reduce the computational cost. Considering that the two-dimensional model requires only 1.7% of the mesh count of a three-dimensional model to accurately capture the gas-liquid interface distribution, the two-dimensional model is adopted to simulate the falling-film flow process. The geometric dimensions of the physical model depicted in Fig. 1 were as follows: the diameter of the liquid distribution opening at the top was 1 mm, and the distance from this opening to the first horizontal tube was 10 mm. To eliminate the influence of the distributor height on the falling-film behavior of the molasses ethanol wastewater, the upper one of the two horizontal tubes (with a diameter of 25.4 mm) was designated as the distribution tube, while the lower one served as the object of simulation.

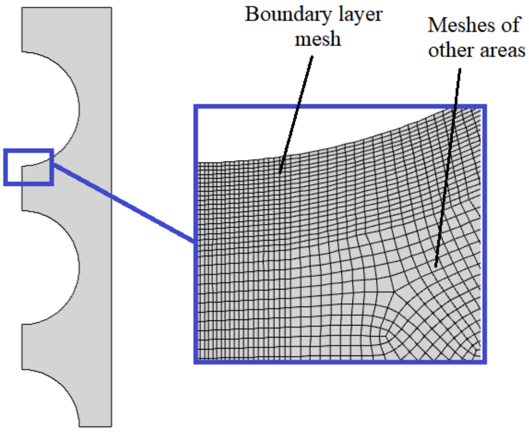

Fig. 1 - Physical model and meshing

As illustrated in Fig. 1, the physical model featured a relatively simple geometry, which was well suited for high-precision structured grids. As the contour of the molasses ethanol wastewater needed to be captured, boundary-layer grids were refined in the near-wall region of the horizontal tubes. The boundary layer comprised 20 layers; the thickness of the first layer was 0.2 mm, and each subsequent layer was 1.15 times as thick as the preceding one. The grid size in the remaining regions was set to 4 mm.

Governing equations

Before establishing the mathematical model, the following assumptions were made regarding the falling-film evaporation of molasses ethanol wastewater *(Wang, 2025)*: (1) the liquid film completely wets the tube surface; (2) only liquid-film flow over the outer surface of the horizontal tube is considered, and the tube wall thickness is neglected; (3) the tube wall temperature is uniform; and (4) the temperature dependence of the thermophysical properties of the molasses ethanol wastewater is neglected.

A numerical model of the falling-film evaporation process was established within an Eulerian framework using the Volume of Fluid (VOF) method. The liquid and gas phases were treated as a single fluid mixture sharing common velocity and pressure fields, and the liquid-gas interface was captured using the phase-volume fraction *(Jia et al., 2026)*.

The transport equation for the liquid-phase volume fraction (α_l), used to capture the liquid-gas interface is expressed as:

$$\frac{\partial \alpha_l}{\partial t} + \nabla \cdot \left(\alpha_l \vec{u} \right) = -\frac{\dot{m}}{\rho_l} \tag{1}$$

The vapor-phase volume fraction (α_v) is given by:

$$\alpha_v = 1 - \alpha_l \tag{2}$$

where: t is the time, s; $\vec{u}$ is the velocity vector, m/s; ρ_l is the density of the molasses ethanol wastewater, kg/m^3; $\dot{m}$ is the volumetric mass-source term associated with evaporation, (kg/(m·s)).

The mixture continuity equation is obtained by summing the mass-conservation equations for the liquid and gas phases *(Jia et al., 2026)*:

$$\frac{\partial \rho}{\partial t}+\nabla\cdot(\rho\vec{u})=0 \tag{3}$$

The density of the fluid mixture (ρ) is calculated as follows:

$$\rho=\alpha_l\rho_l+\alpha_v\rho_v \tag{4}$$

The momentum equation used in the model is given as follows (*Wang, 2025*):

$$\frac{\partial(\rho\vec{u})}{\partial t}+\nabla\cdot(\rho\vec{u}\vec{u})=-\nabla p+\nabla\cdot\left[\mu\left(\nabla\vec{u}+(\nabla u)^T\right)\right]+\rho g+F_\sigma \tag{5}$$

where: p is the pressure, Pa; g is the acceleration due to gravity, m/s^2; μ is the dynamic viscosity of the fluid mixture, Pa·s; F_σ is the surface-tension force per unit volume, N/m^3.

The dynamic viscosity of the fluid mixture is calculated using Eq. (6).

$$\mu=\alpha_l u_l+\alpha_v\mu_v \tag{6}$$

The energy equation is expressed as follows (*Jia et al., 2026*):

$$\frac{\partial(\rho c_p T)}{\partial t}+\nabla\cdot(\rho c_p\vec{u}T)=\nabla\cdot(\lambda\nabla T)-\dot{m}h_v \tag{7}$$

where: c_p is the specific heat capacity of the fluid mixture, J/(kg·K); T is the temperature, K; λ is the thermal conductivity of the fluid mixture, W/(m^2·K); $\dot{m}$ is the mass-transfer rate per unit volume (kg/(m^3·s)); h_v is the latent heat of vaporization, (J/kg).

c_p and μ are calculated using Eqs. (8) and (9).

$$c_p=\alpha_l c_{p,l}+\alpha_v c_{p,v} \tag{8}$$

The phase-change mass-source term is determined using the Lee model:

$$\dot{m}=r_e\alpha_l\rho_l\frac{T-T_{sat}}{T_{sat}} \tag{9}$$

where: r_e is the evaporation relaxation factor, s^{-1}; T_{sat} is the saturation temperature of the molasses ethanol wastewater, ℃;

F_σ in Eq. (5) is calculated using the continuum surface force model proposed by Brackbill (*Yang et al., 2024*):

$$F_\sigma=\sigma\left[\nabla\cdot\left(\frac{\nabla\alpha_l}{|\nabla\alpha_l|}\right)\right] \tag{10}$$

where σ is the surface-tension coefficient at the liquid-gas interface, N/m. The effect of the wall contact angle is incorporated by correcting the interface normal vector near the wall.

The thermophysical properties used in the governing equations are presented in Table 1.

Table 1

Thermal properties parameters

Name	Density / kg/m3	Specific heat capacity/ J/(kg·K)	Thermal conductivity W/(m·K)	Dynamic viscosity / Pa·s
Molasses ethanol wastewater	1096.7	3709	0.58	0.00851
Vapor	0.5542	2014	0.0261	1.34×10-5

Boundary conditions and Simulation Settings

The liquid distribution inlet on the upper side of the horizontal tube is set as a velocity inlet boundary condition, with the velocity set to 0.23 ~ 0.137 m/s to ensure that the spray density remains within the range of 0.010 ~ 0.030 kg/(m·s). The bottom of the horizontal tube is set as a pressure outlet boundary condition with a reference pressure of 0 Pa. The horizontal tube is set as a wall boundary condition, with a constant temperature of 62℃, 64℃, 66℃, and 68℃, respectively, and a contact angle of 60°.

Based on the spray density, the calculated Reynolds number indicates that the investigated Re ranges from 2 to 14, which is far below the turbulent threshold; therefore, in this study, the molasses alcohol waste liquid is considered to exhibit laminar flow.

The numerical simulation is performed using ANSYS Fluent 18.0 software. The pressure and velocity are solved using the Pressure-Implicit with Splitting of Operators (PISO) algorithm. The pressure term is spatially discretized using the PRESTO! scheme, while both the temporal term and the momentum term are discretized using the second-order upwind scheme. In the dynamic time-stepping settings, the maximum Courant number is 0.25.

Evaluations

In falling-film evaporation, the film thickness constituted the dominant thermal resistance during the evaporation process. The degree of uniformity in the film thickness distribution markedly influenced the evaporation rate of the descending liquid film; therefore, it was imperative to examine the film thickness of molasses ethanol wastewater during falling-film evaporation.

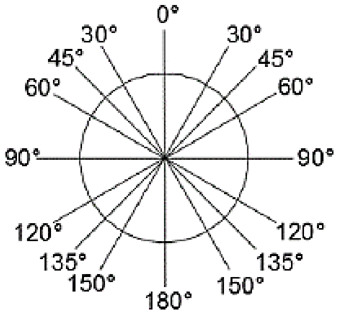

Fig. 2 - Local film thickness measurement method

As illustrated in Fig. 2, with the center of the horizontal tube taken as the origin and the vertically upward direction designated as 0°, straight lines were drawn at circumferential angles of 15°, 30°, 45°, 60°, 75°, 90°, 105°, 120°, 135°, and 150°. The length occupied by the liquid phase along each of these ten lines was extracted directly from Fluent, and this length was defined as the film thickness at the corresponding circumferential angle.

The average heat transfer coefficient served as a pivotal indicator for quantifying the heat transfer rate during the falling-film evaporation of molasses ethanol wastewater, and was determined as follows:

$$h_{ave} = \frac{q}{\Delta T} \tag{11}$$

where: h_{ave} was the average heat transfer coefficient, W/(m^2·K); q was heat flux of the horizontal tube, W/m^2; ΔT was the temperature difference, ℃.

RESULTS AND DISCUSSIONS

Verification

To ensure the relevance of the validation, the experimental cases cited from the literature were selected to closely match the key physical features of the present simulation, including the horizontal tube geometry (D = 25.4 mm), laminar falling-film flow regime, and constant wall-temperature thermal boundary condition. Although the working fluid in the referenced experiments was pure water, the present study focuses on molasses ethanol wastewater, the two fluids have comparable density and surface tension, though the viscosity of the wastewater is moderately higher. This viscosity difference is explicitly accounted for in the present model through the mixture property equations (Eq. (6)). Therefore, the validation results provide meaningful support for the reliability of the present model. Fig.3 presented a comparison between the simulated local film thickness and the experimental ones documented in the literature (*Jia, 2025*). It is evident from Fig.3 that the simulated film thickness conformed to the literature values, both exhibiting an initial thinning followed by a subsequent thickening, with a relative deviation of less than 5%. The falling-film evaporation process constituted a complex heat and mass transfer phenomenon characterized by dynamic coupling between the liquid and gas phases. To further substantiate the validity of the established model, it was necessary to verify its heat transfer characteristics.

Fig. 4 presents the simulated heat transfer coefficient for a smooth tube with the experimental data of *Parken et al.* (*1990*). As clearly observed from Fig. 4, the simulated heat transfer coefficient was in favorable agreement with the values reported in the literature, the relative deviation being below 5%. A synthesis of the analyses in Fig. 3 and Fig. 4 revealed that the developed mathematical model was capable of effectively capturing the physical trends and thermal performance characteristics of molasses ethanol wastewater during falling-film evaporation. It should be noted that, since the validation was performed against external literature data rather than experimental results obtained from the specific molasses ethanol wastewater under identical conditions, the numerical predictions of absolute values may bear inherent uncertainties. Nevertheless, the model demonstrates high reliability in capturing the underlying physical mechanisms and performance trends.

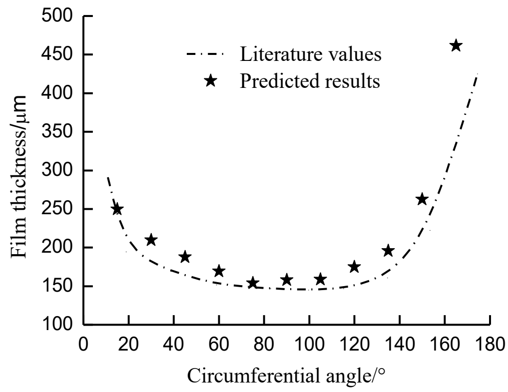

Fig. 3 - Comparison of the reported and simulated film thickness

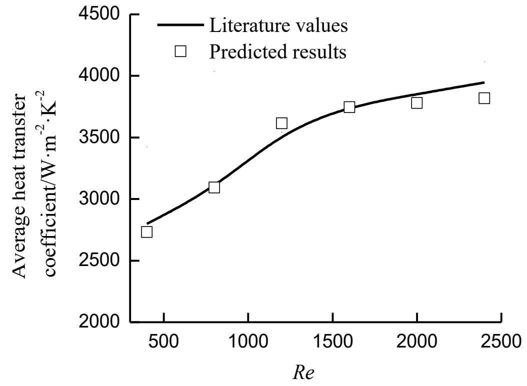

Fig. 4 - Comparison of the reported and simulated average heat transfer coefficient

To ensure the reliability of the numerical results, a systematic mesh-independence study was conducted before the main simulations. Three structured grids were generated with different refinement levels: a coarse mesh (13475 cells), a medium mesh (26669 cells), and a fine mesh (39863 cells). The average heat transfer coefficient and the minimum film thickness at 105° were selected as the evaluation criteria, using a typical operating condition (Γ = 0.20 kg/(m·s), ΔT = 6 °C). The average falling-film heat transfer coefficient decreased from 1724.84 W/(m²·K) for the medium mesh to 1703.72 W/(m²·K) for the finer mesh, with a reduction of only 1.22%. Therefore, the medium mesh can be considered an appropriate meshing scheme.

The effect of spray density

Fig. 5 shows the variation in local liquid film thickness with circumferential angle at spray densities ranging from 0.10 to 0.25 kg/(m·s). Despite differences in spray density, the circumferential distributions of the local film thickness exhibited similar trends. Specifically, as the circumferential angle increased, the film thickness initially decreased, attained its minimum within the circumferential angle of 90° ~ 120°, and subsequently increased.

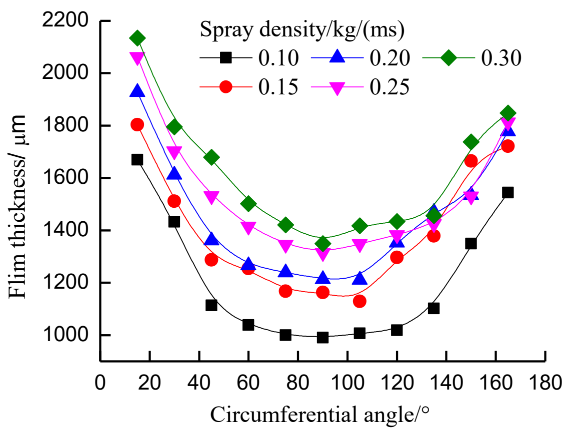

Fig. 5 - Local liquid film thickness at different spray densities

The change behavior of the local film thickness with respect to the circumferential angle conformed to the theoretical prediction derived from Nusselt's classical analysis. Furthermore, it was evident that the local film thickness progressively increased with rising spray density.

The reason was that under gravity, to maintain a steady laminar falling-film, the liquid film had to enlarge its cross-sectional area to handle a greater volumetric flow. An examination of the extent of this influence revealed that when the spray density was augmented from 0.10 to 0.15 kg/(m·s), the film thickness thickened by 16.66%, whereas an increase from 0.25 to 0.30 kg/(m·s) resulted in a mere 5.39% thickening. In accordance with the classical Nusselt laminar falling-film theory, the film thickness scaled with the spray density to the one-third power. Hence, when the spray density already resided within a high baseline range, an identical absolute increment (e.g., 0.05 kg/(m·s)) inevitably induced a pronounced attenuation in the relative increase of the film thickness.

The effect of spray density on the average heat-transfer coefficient is shown in Fig. 6. The average heat transfer coefficient increased monotonically as the spray density increased from 0.10 to 0.30 kg/(m·s), with a relative increase of 23.0% ~ 27.2%. When considered together with the results in Fig. 5, these findings indicate that although increasing the spray density produced a thicker liquid film and consequently increased conductive thermal resistance, the accompanying increase in flow rate raised the film velocity. This enhanced mixing within the liquid film and intensified interfacial disturbances, thereby reducing the thermal-boundary-layer resistance. These results are consistent with those of *Chen et al. (1997)*, who reported an increase in the Nusselt number with increasing film Reynolds number.

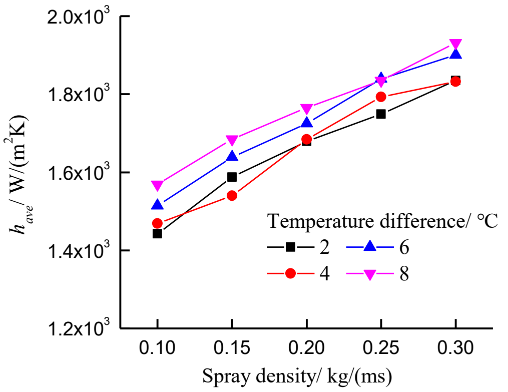

Fig. 6 - Average heat transfer coefficient with spray densities

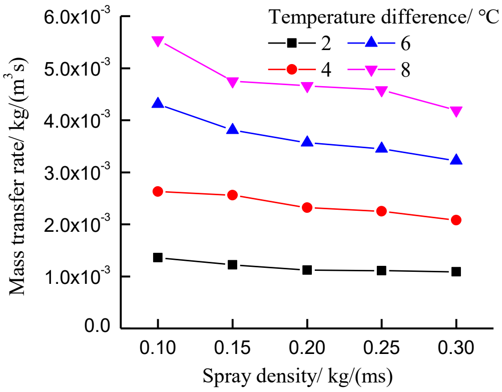

Fig. 7 - Mass volume rate with spray densities

Fig. 7 shows the variation in mass transfer rate with spray density during the falling-film evaporation of molasses ethanol wastewater. The mass transfer rate decreased progressively as the spray density increased. When the spray density increased from 0.10 to 0.30 kg/(m·s), the mass-transfer rate decreased by 19.3% ~ 25.1%. Although the higher flow rate enhanced convective heat transfer, as shown in Fig. 6, the corresponding increase in liquid-film thickness (Fig. 5) increased the heat-transfer distance between the tube wall and the liquid-gas interface. Consequently, the heat supplied at the wall was distributed over a larger liquid volume, reducing the heat available for evaporation per unit volume and thereby decreasing the volumetric mass-transfer rate. Therefore, a relatively low spray density is recommended for enhancing evaporation, provided that complete and stable wetting of the tube surface is maintained.

The effect of temperature difference

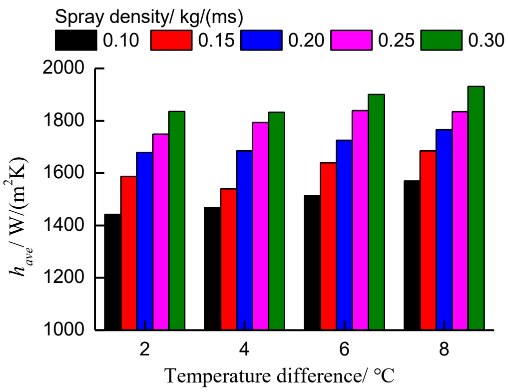

Fig. 8 - Average heat transfer coefficient with temperature difference

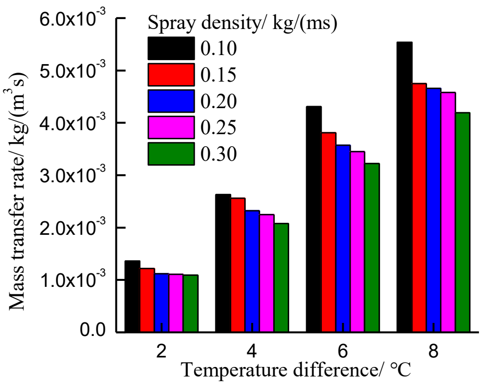

Fig. 9 - Mass volume rate with temperature difference

In addition to spray density, the heat-transfer temperature difference, which is the primary driving force for heat transfer and phase change during falling-film evaporation, requires systematic investigation. Figs. 8 and 9 show the variations in the average heat-transfer coefficient and mass-transfer rate, respectively, during the falling-film evaporation of molasses ethanol wastewater at temperature differences of 2, 4, 6, and 8 °C.

As shown in Fig. 8, the average heat-transfer coefficient increased with increasing temperature difference. At a spray density of 0.10 kg/(m·s), increasing the temperature difference from 2 to 8 °C increased the average heat-transfer coefficient from 1,442.48 to 1,569.14 W/(m²·K), corresponding to a relative increase of 8.8%. The larger temperature difference increased the wall-normal temperature gradient and intensified heat transfer from the inner region of the liquid film toward the liquid–gas interface. The resulting enhancement of evaporation and interfacial disturbance further promoted heat transfer through the liquid film.

As shown in Fig. 9, at a spray density of 0.10 kg/(m·s), increasing the temperature difference from 2 to 8 °C increased the mass-transfer rate from 1.36×10^{-3} kg/(m³·s) to 5.54×10^{-3} kg/(m³·s), with an amplification by a factor of 3.07. Even at the higher spray density of 0.30 kg/(m·s), at which the lowest mass-transfer rates were obtained, the value increased from 1.09×10^{-3} to 4.19×10^{-3} kg/(m³·s), registering a 2.84-fold increase. According to the Lee phase-change model (Eq. (9)), the phase-change mass-source term is positively related to the degree of superheat. As the temperature difference increased, the heat flux from the tube wall to the liquid film increased, allowing the wastewater near the liquid-gas interface to absorb sufficient latent heat and undergo evaporation. These results demonstrate that, within the investigated parameter ranges, increasing the heat-transfer temperature difference was more effective than varying the spray density in enhancing the instantaneous water-removal rate.

To quantitatively compare the relative effects of the two operating parameters, a normalized sensitivity index was defined as $S = (\varphi_{max} - \varphi_{min})/\varphi$. Over the investigated parameter ranges, $S_{\Delta T} = 1.24$, whereas $S_{\Gamma} = 0.11$, indicating that the effect of the heat-transfer temperature difference was approximately 11 times greater than that of spray density. This difference arises because the phase-change mass-transfer rate is directly related to the degree of superheat, whereas spray density affects mass transfer indirectly by altering liquid-film thickness, flow characteristics, and heat-transfer resistance.

CONCLUSIONS

A two-dimensional numerical model of the falling-film evaporation of molasses ethanol wastewater over the outer surface of a horizontal tube was developed using the Volume of Fluid (VOF) method coupled with the Lee phase-change model. The effects of spray density and heat-transfer temperature difference on heat- and mass-transfer performance were systematically investigated. The main conclusions are as follows:

(1) The developed model satisfactorily predicted the liquid-film thickness distribution and heat-transfer characteristics. The simulation results agreed well with experimental data reported in the literature, with relative deviations of less than 5%.

(2) The circumferential distribution of liquid-film thickness was consistent with classical Nusselt theory. As the circumferential angle increased, the film initially became thinner and subsequently thickened, reaching its minimum thickness within the angular range of 90° ~ 120°. Increasing the spray density increased the local film thickness. However, because laminar falling-film thickness is proportional to the cube root of spray density, the rate of film thickening gradually decreased as spray density increased.

(3) Within the spray-density range of 0.10 ~ 0.30 kg/(m·s), the average heat-transfer coefficient increased monotonically with spray density. By contrast, the volumetric mass-transfer rate decreased because the thicker liquid film distributed the supplied heat over a larger liquid volume. Increasing the heat-transfer temperature difference enhanced the thermal driving force, resulting in a moderate increase in the average heat-transfer coefficient and a pronounced increase in the mass-transfer rate. Sensitivity analysis indicated that the effect of temperature difference on the mass-transfer rate was more than one order of magnitude greater than that of spray density.

(4) Within the investigated ranges of spray density (0.10 ~ 0.30 kg/(m·s)) and heat-transfer temperature difference (2 ~ 8 °C), combining a relatively low spray density with a relatively high temperature difference is recommended for the falling-film evaporative concentration of molasses ethanol wastewater. However, the spray density should remain above the critical wetting rate to prevent dry-patch formation. Although a higher temperature difference substantially enhances evaporation, practical applications must also consider heat-source energy consumption and the increased risks of fouling and thermal degradation or carbonization of high-viscosity wastewater on the heated tube surface. Therefore, operating parameters should be comprehensively optimized together with equipment-cleaning intervals.

ACKNOWLEDGMENTS

This work was supported by the Doctoral Research Fund of Shandong Huayu University of Technology and the Shandong Engineering Research Center of Low-Carbon Energy Internet of Things Technology (PT2025KJS004).

REFERENCES

[1] Chen, H., & Jebson, R. S. (1997). Factors affecting heat transfer in falling film evaporators. *Food and Bioproducts Processing*, Vol. 75(2), pp. 111-116, New Zealand.

[2] Chowdhary, P., Raj, A., Bharagava, R.N. (2018). Environmental pollution and health hazards from distillery wastewater and treatment approaches to combat the environmental threats: A review. *Chemosphere*, Vol. 194, pp. 229-246, India.

[3] Dai, Z., Zhang, Y., Wang, S., Nawaz, K., & Jacobi, A. (2022). Falling-film heat exchangers used in desalination systems: A review. *International Journal of Heat and Mass Transfer*, Vol. 185, 122407, Shanghai/ China.

[4] Gong, L. (2017). *Thermal Performance and Parameters Distribution of Large-scale Horizontal-tube Falling Film Evaporators (大型水平管降膜蒸发器热力性能和参数分布特性研究)*. PhD dissertation, Dalian University of Technology, Dalian/ China.

[5] Gong, L., Shen, S., Liu, H. (2016). Parametric distributions of a horizontal-tube falling film evaporator for desalination. *Desalination and Water Treatment*, Vol. 57(25), pp. 11699-11711, Dalian/China.

[6] Ibrahim A., Fath H., Ibrahim M., (2020), Numerical simulation for falling film thickness around horizontal tube in MVC and MED evaporators, *Proceedings of the Materials Science Forum*, pp.139-150, Egypt.

[7] Jia, B. (2025). *Heat Transfer Mechanisms of Droplet Falling Film Evaporation on Nano-structured Surfaces and its Application in Building Wastewater Treatment (纳米结构表面滴状流降膜蒸发传热机理及其在建筑废水处理中的应用)*. Doctoral dissertation, Shandong Jianzhu University, Jinan/China. https://doi.org/10.27273/d.cnki.gsajc.2025.000002

[8] Jia, B., Zhao, Z., Wang, X., Chen, C., Ma, X., Wu, J., Yang, L., Politaeva, N. (2026). Local film thickness in relation to the droplet topological structure of droplet falling film on micro-nano structured horizontal tubes. *Case Studies in Thermal Engineering*, 108125, Dezhou/China.

[9] Jin, P. H., Zhang, Z., Mostafa, I., Zhao, C., Ji, W., Tao, W. (2019). Heat transfer correlations of refrigerant falling film evaporation on a single horizontal smooth tube. *International Journal of Heat and Mass Transfer*, Vol. 133, pp. 96-106, Dalian/China.

[10] Li, J., Xu, J., Ma, N., Tan, C., Xia, Z., Zuo, J. (2022). Research progress on recovery of sugarcane molasses alcohol wastewater (甘蔗糖蜜酒精废液的回收利用研究进展). *Modern Chemical Industry*, Vol. 42(7), pp. 79, Harbin/China. https://doi.org/10.16606/j.cnki.issn0253-4320.2022.07.017.

[11] Liu, S., Mu, X., Shen, S., Li, C., Wang, B. (2021). Experimental study on the distribution of local heat transfer coefficient of falling film heat transfer outside horizontal tube. *International Journal of Heat and Mass Transfer*, Vol. 170, 121031, Dalian/China.

[12] Nusselt, W. (1916). Die Oberflächenkondensation des Wasserdampfes. *Zeitschrift des Vereines Deutscher Ingenieure*, Vol. 60(3), pp. 541-546, 556, Germany.

[13] Parken, W. H., Fletcher, L. S., Sernas, V., Han, J. (1990). Heat transfer through falling film evaporation and boiling on horizontal tubes. *Journal of Heat Transfer*, Vol. 112, pp. 744-750, USA.

[14] Qi, L., Ma, H., Li, C., Luo, Z. (2010). Experimental research on heat transfer performance of falling film evaporation on horizontal tubes (水平管外降膜蒸发传热性能实验研究). *Journal of University of Shanghai for Science and Technology*, Vol. 32(1), pp. 27-30, Shanghai/China. https://doi.org/10.13255/j.cnki.jusst.2010.01.014.

[15] Qiu, Q., Jiang, W., Shen, S., Zhu, X., Mu, X. (2015). Numerical investigation on characteristics of falling film in horizontal-tube falling film evaporator. *Desalination and Water Treatment*, Vol. 55(12), pp. 3247-3252, Dalian/China.

[16] Su, X., & Ouyang, X. (2019). Experimental Study of Falling Film Evaporation Heat Transfer Performance of R410A, R404A and R407C in Horizontal T Type Fin Inner Thread Tube (R410A/R404A/R407C 在 T 型翅内螺纹水平管外的降膜蒸发换热研究). *Journal of Engineering for Thermal Energy and Power*, Vol. 34(2), pp. 88-93, Shanghai/China. https://doi.org/10.16146/j.cnki.rndlgc.2019.02.013

[17] Tahir, F., Mabrouk, A., Koc, M. (2019). Review on CFD analysis of horizontal falling film evaporators in multi effect desalination plants. *Desalination and Water Treatment*, Vol. 166, pp. 296-320, Qatar.
[18] Ubara, T., Asano, H., Sugimoto, K. (2021). Falling film evaporation and pool boiling heat transfer of R1233zd (E) on thermal spray coated tube. *Applied Thermal Engineering*, Vol. 196, 117329, Shanghai/ China.
[19] Wang, D., Shen, S., Pan, B., & Guo, Y. (2026). Numerical study on liquid column deflection and liquid film thickness characteristics of falling film on horizontal tubes under cross-flow steam. *Desalination*, 119884, Dalian/China.
[20] Wang, L. (2025). Numerical simulation on liquid film flow turbulence characteristics of corrugated baffle-type plate under high Reynolds number. *Chemical Engineering and Processing-Process Intensification*, 110511, Shanghai/China.
[21] Wang, L., Huang, X., Wang, Y., Yu, G. (2026). Study on falling film in large-diameter tube and co-current gas-liquid heat transfer under high temperature and velocity of gas flow. *Chemical Engineering Research and Design*, Vol. 225, pp. 230-244, Shanghai/China.
[22] Yang, L., Jia, B., Zhang, Q., Zhou, Z. (2024). Effect of dynamic contact angle behavior on droplet topological structure and film thickness evolutions in droplet mode. *Desalination*, Vol. 576, 117359, Jinan/China.
[23] Zhang, Y., Wang, D., Liu, Y., Tang, M., Zhang, S. (2020). Distribution characteristics of falling film thickness around a horizontal corrugated tube [J]. *International Journal of Heat and Mass Transfer*, 154: 119773, Tianjin/China.
[24] Zhao, C., Ji, W., Jin, P., Zhong, Y, Tao, W. (2018). Hydrodynamic behaviors of the falling film flow on a horizontal tube and construction of new film thickness correlation. *International Journal of Heat and Mass Transfer*, Vol. 119, pp. 564-576, Hangzhou/China.